ISSN 1064-2269, Journal of Communications Technology and Electronics, 2016, Vol. 61, No. 6, pp. 630–638. © Pleiades Publishing, Inc., 2016.
Original Russian Text © P.V. Mazaev, V.V. Koledov, V.G. Shavrov, P.V. Lega, A.V. Mashirov, A.P. Kamantsev, D.S. Kuchin, D.V. Kolesov, I.V. Yaminskii, D.I. Zakharov, V.A. Dikan, A.V. Irzhak, 2016, published in Radiotekhnika i Elektronika, 2016, Vol. 61, No. 6, pp. 593–601.

PHYSICAL PROCESSES IN ELECTRON DEVICES

Thermoelastic Properties of Micron-Size Actuators Based on the Ti_2NiCu/Pt Composite with Shape-Memory Effect

P. V. Mazaev[a], V. V. Koledov[a], V. G. Shavrov[a], P. V. Lega[a], A. V. Mashirov[a], A. P. Kamantsev[a], D. S. Kuchin[a], D. V. Kolesov[b], I. V. Yaminskii[b], D. I. Zakharov[c], V. A. Dikan[c], and A. V. Irzhak[c, d]

[a] *Kotel'nikov Institute of Radio Engineering and Electronics, Russian Academy of Sciences, Mokhovaya ul. 11, str. 7, Moscow, 125009 Russia*

[b] *Moscow State University, Moscow, 119991 Russia*

[c] *National Research Technological University MISiS, Leninskii pr. 4, Moscow, 119049 Russia*

[d] *Institute of Microelectronic Technology and Ultrahigh-Purity Materials, Russian Academy of Sciences, ul. Akademika Osip'yana 6, Chernogolovka, Moscow oblast, 142432 Russia*

e-mail: victor_koledov@mail.ru, lega_peter@list.ru

Received December 22, 2014

Abstract—Thermomechanical properties of microactuators with shape-memory effect (SME) based on the Ti_2NiCu/Pt layered composite are analyzed. Atomic-force microscopy is used to experimentally determine rigidity of the composite microactuators that represent cantilevers with sizes of $50 \times 2 \times 1$ μm and a thickness of the SME active alloy layer of 0.5 μm in a temperature interval of 20–100°C. Forces that are exerted by the composite actuator on a microscopic object are quantitatively estimated. The experimental data are in reasonable agreement with the calculated results.

DOI: 10.1134/S1064226916060176

INTRODUCTION

Nanotechnological objects that exhibit new physical properties are extensively employed in modern industry. Manipulation of nanosized objects necessitates the development of micromechanical devices based on various physical principles. Note systems for manipulation of micro- and nanosized objects that are based on bimorph composites consisting of an alloy with shape-memory effect (SME) and an elastic layer. Figure 1 shows the composite SME nanotweezers of [1–8]. A specific feature of the SME alloys lies in gigantic (up to 10%) deformation related to the thermoelastic martensite transition caused by variations in temperature or magnetic field [9–18]. Functional materials based on the SME alloys can be used to produce mechanical manipulation systems with sizes comparable with the sizes of nanoscale objects (e.g., carbon nanotubes (CNTs), nanotubes, various nanoparticles, etc.).

Figure 2 presents the working principle of the composite SME microactuator. The application of a two-layer composite consisting of a preliminary extended alloy with single-side SME and an elastic layer makes it possible to obtain controlled deformation even in the absence of specific training of alloy with respect to the two-side SME. The bending is reached due to the SME upon heating, and the restoration of the original shape is provided by the elastic layer upon cooling.

The advantages of the above configuration are as follows: simplicity of structure, manufacturability, record-small sizes, and convenient interval of activation temperature (20–60°C) that allows manipulation

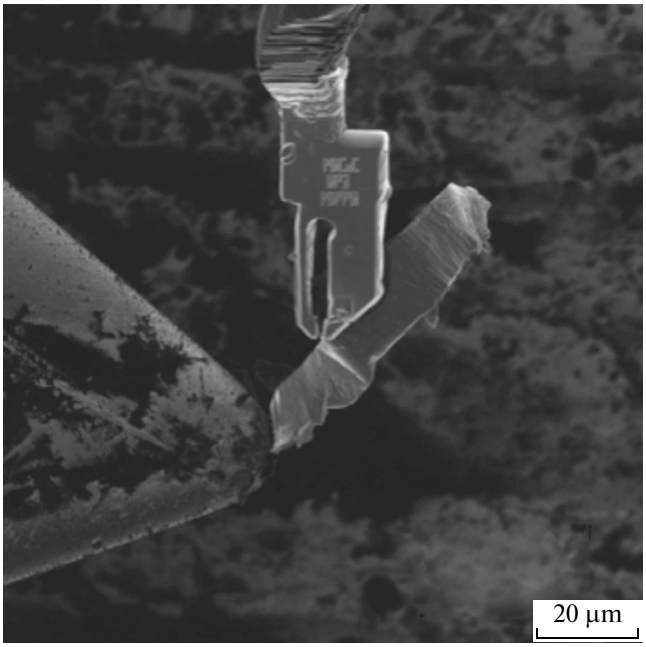

Fig. 1. Nanotweezers based on the SME composite.

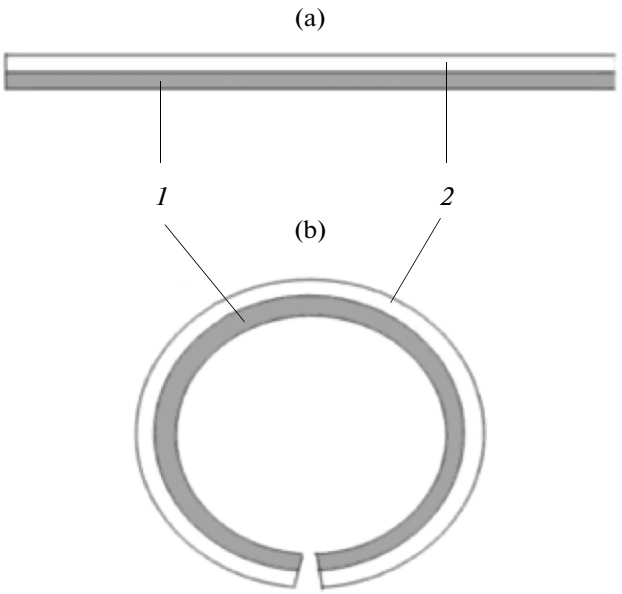

Fig. 2. Working principle of the SME composite: (*1*) SME alloy layer and (*2*) elastic layer in (a) undeformed composite (prior to heating) and (b) bent composite (after heating).

of even biological objects. Manipulation of microscopic objects with the aid of nanotweezers necessitates the analysis and control of the corresponding forces. However, nanotweezers also represent microscopic objects and, as was mentioned, conventional methods for the measurement of elastic properties are missing.

The purpose of this work is the quantitative estimation of the forces exerted by the composite microactuator of nanotweezers on the object under study. To solve such a problem, we propose a method for the measurement of the temperature dependence of the rigidity of microactuator based on the methods for the measurement of the rigidity of cantilevers in scanning probe microscopy (SPM).

1. EXPERIMENTAL METHOD

Rigidity of cantilevers must be measured and calibrated in practical SPM [19, 20]. Existing methods for calibration can be used owing to the similarity of the shape and sizes of microactuators and rectangular SPM cantilevers. A method of reference cantilever is employed in [20] for the calibration of SPM cantilevers (Fig. 3). Such a method is used to calibrate a cantilever with unknown rigidity constant with the aid of the load–displacement curve and accurately calibrated reference cantilever *2* that is contact with the cantilever under study (*1*).

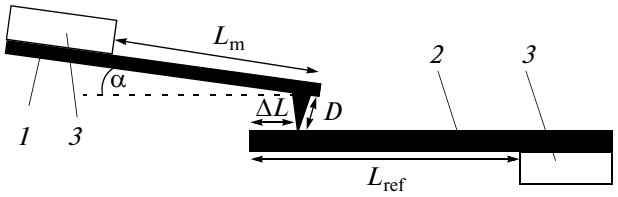

Fig. 3. Experimental model of the measurements using reference cantilever: (*1*) measured cantilever, (*2*) reference cantilever, and (*3*) silicon chips.

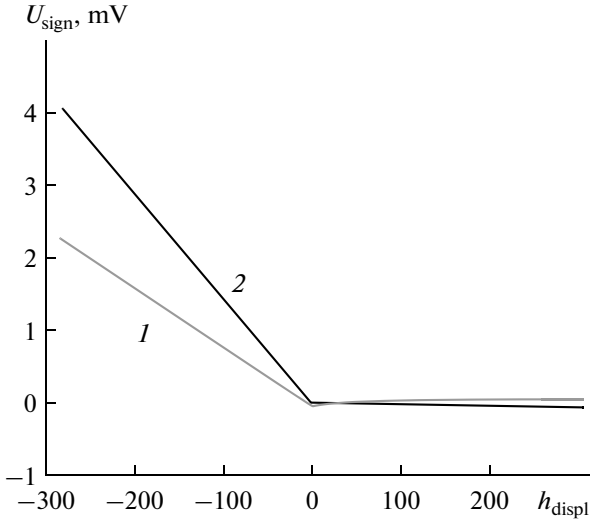

Fig. 4. Load–displacement curves for the interaction of the measured cantilever and (*1*) solid surface and (*2*) reference cantilever (U_{sign} is the photodetector signal and h_{displ} is the displacement of translation stage) [19].

The rigidity of the measured cantilever is given by [20]

$$k_m = k_{ref}\left(\frac{(S_t)_{ref\,m}}{(S_t)_{ref\,s}} - 1\right)\left(1 - \left(\frac{3D}{2L_m}\right)\tan\alpha\right) \times \left(\frac{L_{ref}}{L_{ref} - \Delta L}\right)^3 \cos^2\alpha, \quad (1)$$

where k_{ref} is the rigidity constant of the reference cantilever, $(S_t)_{ref\,s}$ is the averaged inverse slope of the load–displacement curve (e.g., in nm/mV) that is obtained for the measured cantilever loaded on solid surface (e.g., silicon chip), $(S_t)_{ref\,m}$ is the averaged inverse slope of the load–displacement curve that is obtained for the interaction of the measured and reference cantilevers (Fig. 4), D is the tip height of the measured cantilever, L_m is the length of the measured cantilever from the base to the tip, L_{ref} is the length of the reference cantilever, and ΔL is the distance from the end of the refer-

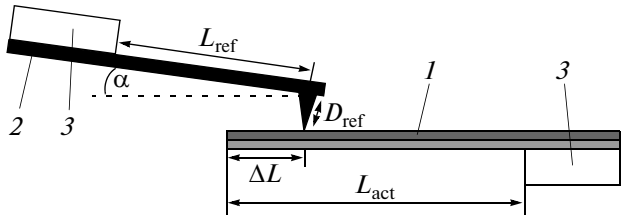

Fig. 5. Scheme of the method of inverted reference cantilever: (*1*) measured cantilever, (*2*) reference cantilever, and (*3*) silicon chips.

ence cantilever to the point of contact with the measured cantilever.

A factor of $\cos^2\alpha$ is introduced in formula (1), since cantilever k_m can be placed at angle α to the surface, which is typical of the SPM structures. A factor of $\left(1-\left(\frac{3D}{2L_m}\right)\tan\alpha\right)$ is responsible for the torque related to the tip height. We may assume that such a factor is unity under the condition $D \ll L_m$. A factor of $\left(\frac{L_{ref}}{L_{ref}-\Delta L}\right)^3$ is needed, since the rigidity of the reference cantilever increases with a decrease in the length of the arm of beam:

$$k_{\Delta L}^{ref} = k_L^{ref}\left(\frac{L_{ref}}{L_{ref}-\Delta L}\right)^3, \quad (2)$$

where k_L^{ref} and $k_{\Delta L}^{ref}$ are the rigidities of the reference cantilevers with lengths L_{ref} and $L_{ref}-\Delta L$, respectively.

Equation (1) establishes a relationship of rigidity coefficients of the reference and measured cantilevers. When the reference cantilever serves as the upper cantilever and the microactuator under study serves as the lower cantilever, the rigidity coefficient can be determined using the method of inverted reference cantilever. In this case (Fig. 5), the rigidity coefficient of microactuator is written as

$$k_{act} = k_{ref}\left[\left(\frac{S_{ac}}{S_s}-1\right)\left(1-\left(\frac{3D_{ref}}{2L_{ref}}\right)\tan\alpha\right)\cos^2\alpha\right]^{-1} \times\left(\frac{L_{act}}{L_{act}-\Delta L}\right)^{-3}, \quad (3)$$

where S_{ac} is the averaged inverse angular coefficient of the load–displacement linear dependence (e.g., in nm/mV) that is obtained for the interaction of the microactuator and reference cantilever, S_s is the averaged inverse angular coefficient of the load–displacement linear dependence that is obtained for the reference cantilever loaded on solid surface (e.g., silicon chip), D_{ref} is the tip height of the reference cantilever, L_{act} is the length of microactuator, and ΔL is the distance from the end of the microactuator to the point of contact with the reference cantilever.

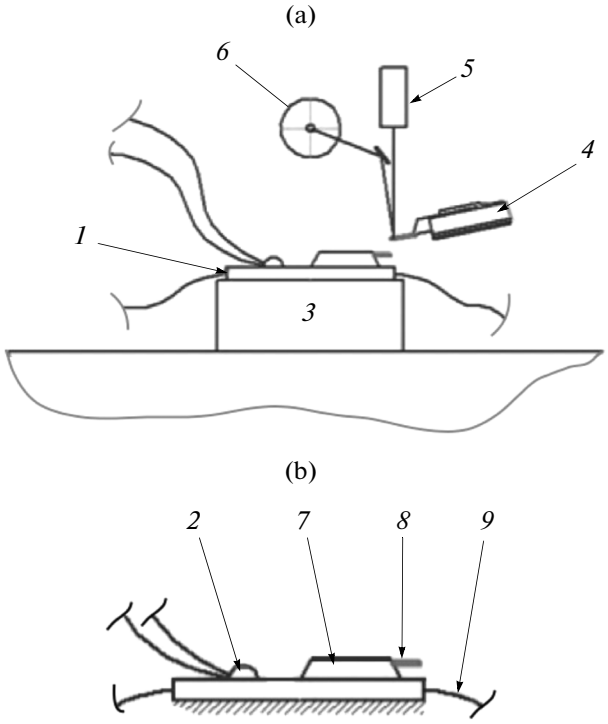

Fig. 6. (a) General scheme of experimental setup and (b) scheme of the heating table: (*1*) heater, (*2*) thermocouple, (*3*) SPM base, (*4*) holder of the SME head, (*5*) laser, (*6*) photodetector, (*7*) silicon chip, (*8*) actuator, and (*9*) contacts of heater and thermocouple.

2. EXPERIMENTAL SETUP

The experimental setup for implementation of the above procedure for the measurement of the rigidity of the SME microactuator versus temperature is based on a FemtoSkan SPM [21]. The setup (Fig. 6) contains heater *1* and thermocouple *2* that are mounted on SPM base *3*. The reference cantilever is fixed in holder *4* of the SPM head that is placed above the heater. Beam of laser *5* is reflected from the reference cantilever to photodetector *6*. Silicon chip *7* with fixed microactuator *8* is placed on heater *1*. Contact of microactuator *8* and cantilever is provided when the sample stage is roughly or accurately moved toward the probe. Rough and accurate displacements are provided by a stepper motor and piezoceramic tube, respectively.

3. EXPERIMENTAL SAMPLES

Bimetal composite microactuators are made of fast-quenched Ti_2NiCu SME alloy that is fabricated as ribbons with the aid of spinning. The temperatures at which the direct and reverse martensite transformations are started and ended range from 40 to 80°C

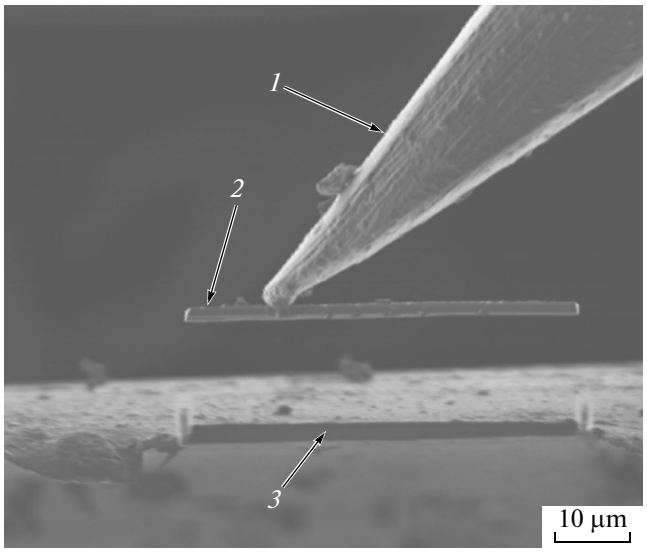

Fig. 7. Transportation of microactuator using an OmniProbe manipulator in the FIB chamber: (*1*) OmniProbe manipulator, (*2*) microactuator, and (*3*) ribbon of the Ti_2NiCu SME alloy.

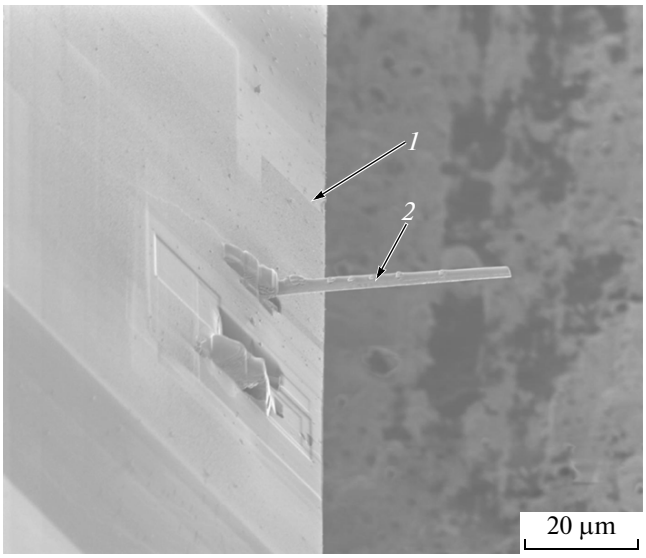

Fig. 8. Image of the first microactuator: (*1*) silicon chip and (*2*) microactuator.

[3, 4]. The preliminary deformation of the ribbon is $\Delta\varepsilon_0 = 0.01$. The production technology and properties of the fast-quenched Ti_2NiCu alloy can be found in [3, 5].

The microactuators are fabricated using selective ion etching, and the elastic platinum layer is deposited with the aid of ion-stimulated vapor deposition. The production technology of the Ti_2NiCu/Pt composite can be found in [4, 6]. The fabrication of experimental samples of microactuators in the chamber of the device with focused ion beam (FIB) (an FEI StrataFIB 201 ion microscope) consists of the following stages.

(i) Fabrication of an elastic layer of metal platinum on the surface of preliminary stretched fast-quenched ribbon made of the Ti_2NiCu SME alloy using the ion-stimulated deposition of platinum.

(ii) Formation of a bimetal beam of the composite microactuator from the fast-quenched Ti_2NiCu alloy in the FEI StrataFIB 201 setup with the aid of selective ion etching using gallium ions.

(iii) Detachment and transportation of microactuator to a silicon chip using an OmniProbe manipulator in the FEI StrataFIB 201 setup (Fig. 7).

A series of three microactuators has been fabricated using such a technology (Table 1). Absolute thicknesses and thickness ratios of the microactuator layers depend on the rate of ion-stimulated deposition of FIB. Figure 8 shows the image of the first microactuator.

4. EXPERIMENT

When the heater with the sample is placed on the SPM base, the microactuator is roughly shifted toward the cantilever. Accurate displacement is used at a distance of about 50 μm between the microactuator and cantilever. The corresponding position is assumed to be the initial position in the experiment (Fig. 9a). Accurate displacement is performed up to the moment of contact of the microactuator and cantilever (Fig. 9b). The moment of contact is determined using the signal of photodiode and is visually monitored using an optical microscope. Then, the translation stage moves under computer control (Fig. 9c) along the vertical axis by several micrometers. Such a motion leads to the deformation of the microactuator and cantilever and causes variation in the photodiode signal, so that the dependence of the photodiode signal on the position of the translation stage is obtained. When the dependence is obtained, the translation stage is shifted to the initial position at a distance of about 50 μm (Fig. 9d) and the temperature of heater is changed (Fig. 9e). Then, the procedure is repeated.

Table 1. Sizes of the three microactuators

Sample	Length, μm	Width, μm
1	45 ± 0.5	2.4 ± 0.1
2	51 ± 0.5	2.5 ± 0.1
3	43 ± 0.5	1.9 ± 0.1

The thickness of each sample is about 1, and the thickness ratio of elastic and SME layers is about 1 : 1.

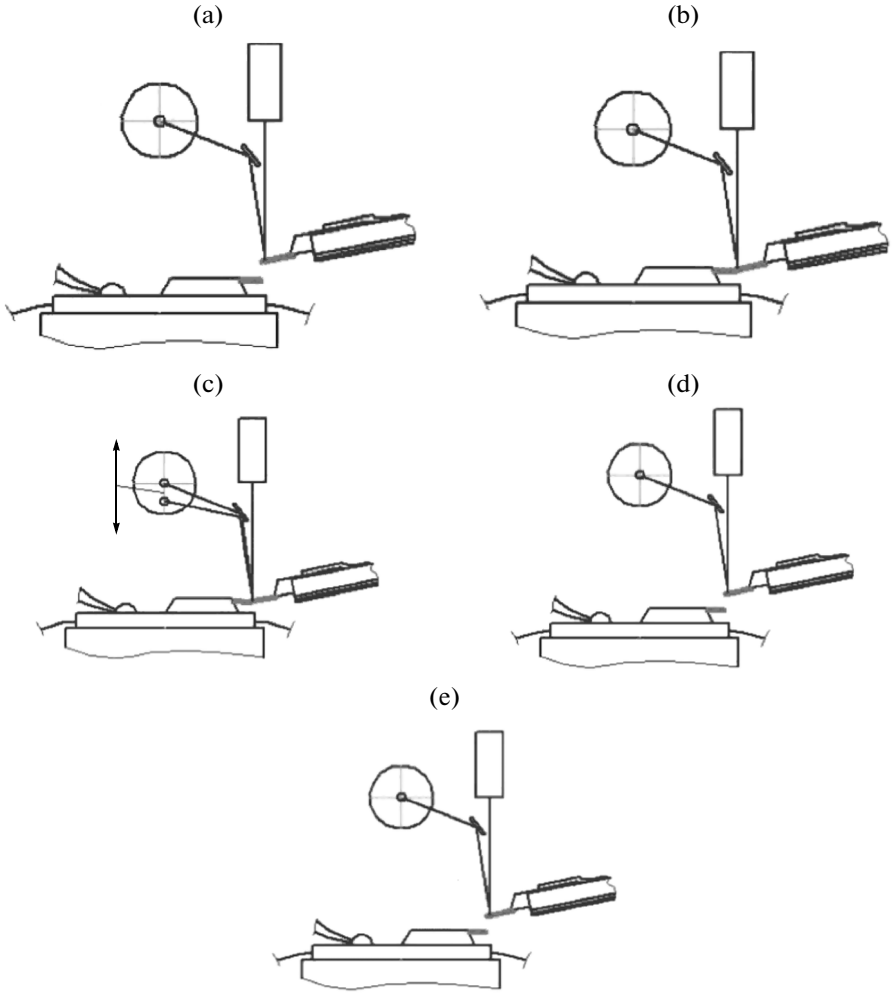

Fig. 9. Scheme of experiment: (a) initial position, (b) moment of contact, (c) measurement of rigidity and calculation of the dependence, and (d) motion to the initial position at $t = t_0$ and (e) an increase in temperature to $t = t_0 + t$.

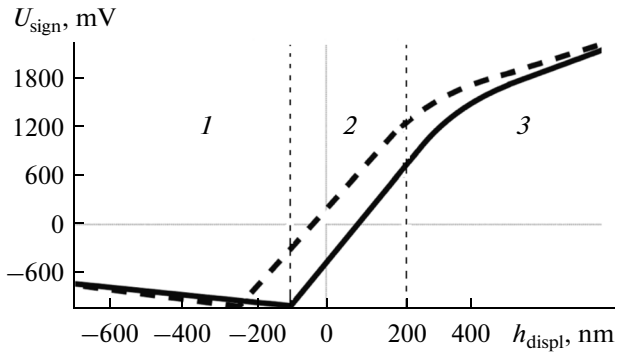

Fig. 10. Typical plot of signal vs. displacement of translation stage: (*1*) region in which the microactuator approaches the cantilever, (*2*) linear interaction, and (*3*) excess bending of cantilever.

Figure 10 presents a typical dependence of signal U_{sign} that is obtained for the upward and, then, downward motion of the translation stage. Three main regions can be determined for the upward motion.

Region 1 is the region in which the microactuator moves toward the cantilever and the direct contact is absent. We observe a negative slope of the curve related to the mutual attraction of the microactuator and cantilever prior to the contact.

Region 2 is the region of the linear dependence of the photodiode signal on the displacement that is obtained due to the mechanical contact of the microactuator and cantilever. The laser beam reflected from elastically bent cantilever is shifted along the aperture of the differential photodetector, and a linear dependence of the signal on the displacement of the translation stage is obtained.

Table 2. Rigidity coefficient $k_{act\,i}$ versus temperature T for the three microactuators

No. 1		No. 2		No. 3	
T, °C	$k_{act\,1}$, N/m	T, °C	$k_{act\,2}$, N/m	T, °C	$k_{act\,3}$, N/m
Heating					
22	6.35 ± 0.450	26	1.39 ± 0.146	25	1.72 ± 0.203
39	7.65 ± 0.702	40	1.05 ± 0.281	42	1.74 ± 0.663
48	8.61 ± 0.691	56	0.72 ± 0.075	52	1.38 ± 0.406
91	3.13 ± 0.472	91	0.85 ± 0.038	61	1.30 ± 0.356
–	–	–	–	75	1.06 ± 0.200
–	–	–	–	86	0.97 ± 0.163
Cooling					
–	–	69	0.89 ± 0.107	69	0.75 ± 0.030
–	–	54	0.72 ± 0.048	60	0.87 ± 0.142
–	–	36	0.74 ± 0.093	47	0.92 ± 0.160
–	–	26	0.76 ± 0.166	39	1.18 ± 0.352
–	–	–	–	35	1.39 ± 0.178
–	–	–	–	28	1.18 ± 0.085
–	–	–	–	22	1.35 ± 0.114
Reheating					
–	–	–	–	51	1.07 ± 0.032
–	–	–	–	75	1.04 ± 0.398

Region 3 is the saturation region in which the linearity of the dependence is violated, since significant bending of the cantilever leads to such a deflection of the laser beam at which is leaves the aperture of the photodetector.

Region 2 is the characteristic region in which the rigidity of the microactuator can be studied.

4.1. Data Analysis

The main task of the data analysis is the selection of the linear fragment of the curve and calculation of the inverse angular coefficient measured in nm/mV. Then, the result is substituted in formula (3) as coefficient S_{ac}.

We assume that a factor of $\left(1-\left(\frac{3D_{ref}}{2L_{ref}}\right)\tan\alpha\right)$ in formula (3) is unity, since the tip length of the reference cantilever is $D_{ref} = 0$. A constant angle of 12° is established between the cantilever and microactuator in the FemtoSkan SPM. Thus, formula (3) is represented as

$$k_{act} = k_{ref}\left[\left(\frac{S_{ac}}{S_s}-1\right)\cos^2\alpha\right]^{-1}\left(\frac{L_{act}}{L_{act}-\Delta L}\right)^{-3}. \quad (4)$$

First, we determine inverse angular coefficient S_s that is obtained when the cantilever acts upon the solid surface of silicon chip.

4.2. Calibration of Cantilever on Solid Surface

The cantilevers are calibrated at room (22°C) and high (90°C) temperatures and inverse angular coefficients of S_s = 0.149 ± 0.00359 and 0.179 ± 0.00351 nm/mV, respectively, are obtained.

The results show that an increase in temperature by 60–70°C leads to an increase in coefficient S_s by 15–20% due to a variation in the rigidity of cantilever, changes of the characteristics of the FemtoSkan SPM, and instability of the vertical position of solid substrate owing to the temperature drift.

5. EXPERIMENTAL RESULTS

Experimental inverse angular coefficients S_{ac} are averaged and substituted in formula (4). The results are used to calculate rigidity coefficients of microactuators k_{act} (Table 2).

At a temperature of higher than 80°C, the rigidity of microactuators decreases by a factor of about 2. Friction at the contact point of cantilever and microactuator and the temperature drift lead to the nonlinearity of the dependence with local maxima and minima. Figure 11 shows the most typical dependence for the third microactuator.

Note that the end point of microactuator is approached in the horizontal plane with a step of 2 μm. Therefore, the experimental rigidities correspond to the microactuator lengths decreased by ΔL = 2 μm.

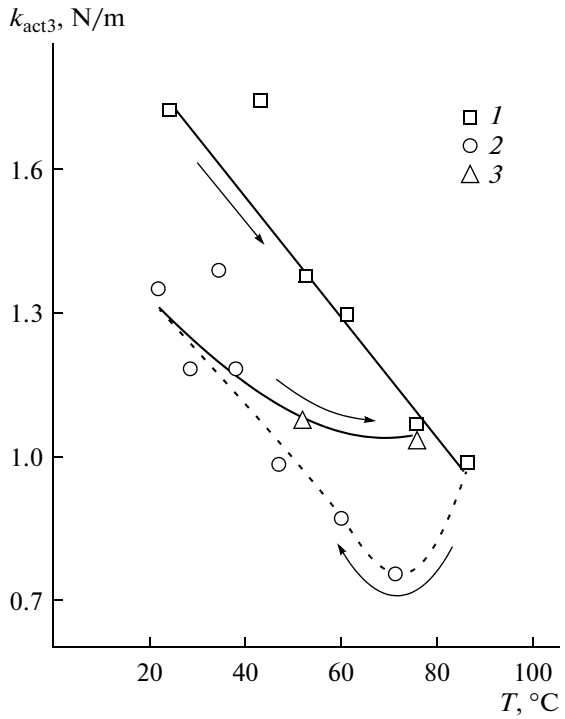

Fig. 11. Plots of rigidity coefficient $k_{act\,3}$ of the third microactuator vs. temperature T: (*1*) heating, (*2*) cooling, and (*3*) reheating. The dots show the mean values at the given temperature and the arrows show temperature variations. The mean relative error is 18.7%.

6. DISCUSSION OF THE MEASURED RIGIDITIES

The experimental data show that the cantilever rigidity decreases by 49–74% when the temperature increases. In spite of a random error in the experiments and difficulties related to establishing of identical contacts of microactuator and cantilever, such a tendency is valid for all samples. This result can be due to a decrease in the elasticity modulus of the materials of cantilever and microactuator and structural transformations of the composite microactuator (e.g., austenite transition of the Ti_2NiCu alloy due to heating). To specify the reasons for a decrease in the rigidity of microactuator upon heating, we must additionally determine the rigidities of layers of the composite microactuator using the corresponding samples, analyze the rigidity of the composite microactuator in the presence of stresses directed along and oppositely to the direction of the internal moment resulting from the reverse martensitic transition and along the perpendicular direction.

7. THEORETICAL ESTIMATION OF THE FORCE EXERTED BY MICROACTUATOR ON OBJECT

The theory of the composite actuator [7] yields a formula that makes it possible to calculate the force

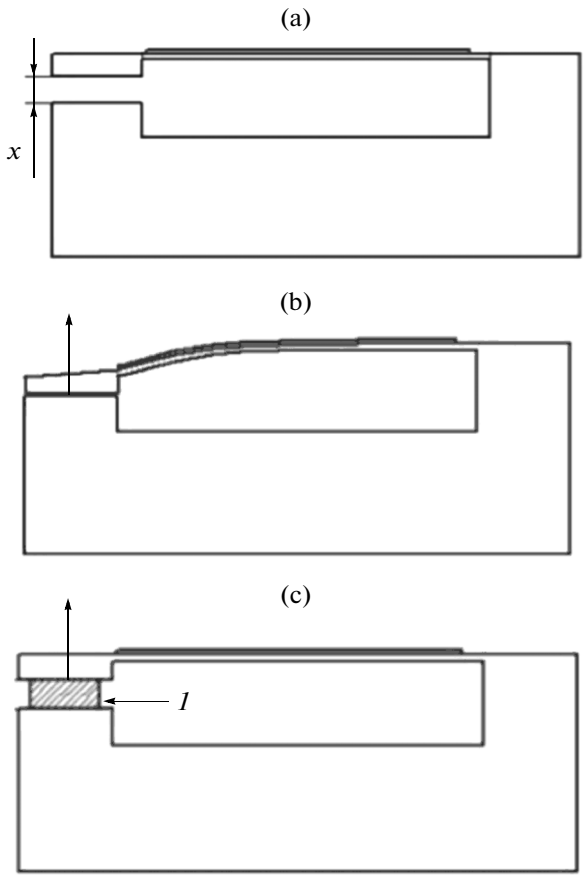

Fig. 12. Simplest calculation of the microactuator force: (a) room temperature, (b) high temperature and zero force ($F_{exp} = 0$ N), and (c) high temperature and a force of $F_{exp} = xk_{act}$ (x is the size of sample *1*).

exerted by the actuator when the activation and reverse martensitic transition take place at fixed composite:

$$F_{theor} = \frac{Ebh^2}{2l(1-\Delta\varepsilon_0)}\Delta\varepsilon_0. \quad (5)$$

Here, E is the elasticity modulus of microactuator and b, h, and l are the microactuator width, thickness, and length, respectively.

The microactuator consists of two layers (Ti_2NiCu SME layer and elastic platinum layer), so that reduced elasticity modulus E_r that takes into account the properties of both materials must be employed [22]:

$$E_r = \frac{4E_{Ti_2NiCu}E_{Pt}}{\left(\sqrt{E_{Ti_2NiCu}} + \sqrt{E_{Pt}}\right)^2}. \quad (6)$$

Using $E_{Pt} = 168$ GPa and $E_{Ti_2NiCu} \approx 70$ GPa (for austenite), we obtain $E_r \approx 103$ GPa.

Table 3. Calculation of forces for the three actuators

No.	x, mm	F_{exp}, μN	F_{theor}, μN	k_{act}, N/m	k_{act}^{theor}, N/m
1	7.6	23.8	27.6	3.13	3.64
2	9.8	8.3	25.4	0.85	2.60
3	6.9	6.7	22.9	0.97	3.30

The bending of microactuator due to reverse martensitic transition can be calculated using the formula of [7]:

$$x = \frac{3l^2}{8h}\Delta\varepsilon_0. \quad (7)$$

We assume that the force exerted on the fixed part of the tweezers is zero when the temperature is higher than the point of the martensite–austenite transition and the complete bending of the microactuator is reached (Fig. 12). Then the following force is exerted on object *1* with thickness x that is pressed between the fixed part of tweezers and microactuator:

$$F_{exp} = xk_{act}. \quad (8)$$

To compare the theoretical and experimental results, we calculate theoretical rigidity k_{act}^{theor}:

$$k_{act}^{theor} = \frac{F_{theor}}{x} = \frac{4Ebh^3}{3l^3(1-\Delta\varepsilon_0)}. \quad (9)$$

Table 3 presents the theoretical results that are in reasonable agreement with the experimental data.

Nanotweezers must be constructed with allowance for both the size of object under study and the force exerted on such an object. For example, fragility of various bacteria (spores and vegetative form) has been studied in [23, 24] under an external force of about one micronewton. Bacteria may be destroyed or exhibit integrity in the presence of such a force. To solve the problems, we must preliminary calculate bending x and desired rigidity taking into account the sizes of object and parameters of nanotweezers (E, b, h, and l).

CONCLUSIONS

We have developed a method to study thermoelastic properties of microscopic samples in a temperature interval of 20–100°C with the aid of a FemtoSkan SPM. Selective ion etching is used to fabricate samples of composite microactuators based on Ti_2NiCu/Pt with SME and platinum layer thicknesses of about 500 nm, a length of 45–51 μm, and a width of 1.9–2.5 μm.

The temperature dependence of the elastic properties of composite microactuators is studied in a temperature interval of 22–91°C. A monotonic decrease in rigidity coefficient k_{act} [N/m] versus temperature is revealed and variations in quantity k_{act} are demonstrated (Table 3). Several effects leading to a decrease in the rigidity upon heating are analyzed.

The forces generated by microactuators are calculated. Within experimental error, the measured rigidities coincide with the calculated results on the assumption that the properties of original materials remain unchanged at submicron thicknesses.

Based on the experimental rigidities, we calculate the force of microtweezers that is exerted on micro- and nanosized objects. For the microactuators under study, such a force ranges from 6.1 to 21.7 μN.

ACKNOWLEDGMENTS

This work was supported by the Russian Science Foundation (project no. 14-19-01644).

REFERENCES

1. A. Irzhak, V. Koledov, D. Zakharov, et al., J. Alloys Compd. **586** (Suppl. 1), S464 (2014).
2. S. P. Belyaev, N. N. Resnina, A. V. Irzhak, et al., J. Alloys Compd. **586** (Suppl. 1), 222 (2014).
3. A. V. Shelyakov, N. N. Sitnikov, V. V. Koledov, et al., Int. J. Smart Nano Materials **2** (2), 68 (2011).
4. D. Zakharov, G. Lebedev, A. Irzhak, et al., Smart Materials Structures **21**, 052001 (2012).
5. A. V. Shelyakov, N. N. Sitnikov, A. P. Menushenkov, et al., Thin Solid Films **519**, 5314 (2011).
6. D. Zakharov, G. Lebedev, V. Koledov, et al., Phys. Procedia **10**, 58 (2010).
7. A. V. Irzhak, D. I. Zakharov, V. S. Kalashnikov, V. V. Koledov, D. S. Kuchin, G. A. Lebedev, P. V. Lega, E. P. Perov, N. A. Pikhtin, V. G. Pushin, I. S. Tarasov, V. V. Khovailo, V. G. Shavrov, and A. V. Shelyakov, J. Commun. Technol. Electron. **55**, 818 (2010).
8. A. V. Irzhak, V. S. Kalashnikov, V. V. Koledov, D. S. Kuchin, G. A. Lebedev, P. V. Lega, N. A. Pikhtin, I. S. Tarasov, V. G. Shavrov, and A. V. Shelyakov, Tech. Phys. Lett. **36**, 329 (2010).

9. A. D. Bozhko, A. N. Vasil'ev, V. V. Khovailo, et al., JETP Lett. **67** (3), 227 (1998).
10. A. Vasil'ev, A. Bozhko, V. Khovailo, et al., J. Magn. Magn. Mater. **196–197**, 837 (1999).
11. V. Buchelnikov, I. Dikshtein, R. Grechishkin, et al., J. Magn. Magn. Mater. **272–276**, 2025 (2004).
12. I. Dikshtein, V. Koledov, V. Shavrov, et al., IEEE Trans. Magn. **35**, 3811 (1999).
13. N. I. Kourov, A. V. Korolev, V. G. Pushin, et al., Phys. Met. Metallogr. **99** (4), 376 (2005).
14. V. G. Pushin, N. I. Kourov, A. V. Korolev, et al., Phys. Met. Metallogr. **99**(4), 401 (65).
15. I. E. Dikshten, D. I. Ermakov, V. V. Koledov, L. V. Koledov, T. Takagi, A. A. Tulakova, A. A. Cherechukin, and V. G. Shavrov, JETP Lett. **72**, 373 (2000).
16. A. A. Cherechukin, I. E. Dikshtein, D. I. Ermakov et al., Phys. Lett. A **291** (2–3), 175 (2001).
17. E. Kalimullina, A. Kamantsev, V. Koledov, et al., Phys. Status Solidi **11**, 1023 (2014).
18. V. D. Buchel'nikov, A. N. Vasil'ev, V. V. Koledov, et al., PHYSICS-USPEKHI **49**, 871 (2006).
19. R. S. Gates and M. G. Reitsma, Rev. Sci. Instrum. **78**, 086101 (2007).
20. A. D. Slattery, A. J. Blanch, J. S. Quinton, and C. T. Gibson, Nanotecnology **24**, 015710 (2013).
21. http://www.nanoscopy.ru/equipment/femtoscan/
22. S. D. Ponomarev and L. E. Andreeva, *Calculation of Elastic Elements of Machines and Devices* (Mashinostroenie, Moscow, 1962) [in Russian].
23. A. V. Bolshakova, O. I. Kiselyova, A. S. Filonov, et al., Ultramicroscopy **86** (1–2), 121 (2001).
24. A. V. Bolshakova, O. I. Kiselyova, and I. V. Yaminsky, Biotechnol. Progress **20**, 1615 (2004).

Translated by A. Chikishev